coatings

MDPI

Article

$Co_{0.6}Ni_{0.4}S_2$/rGO Photocatalyst for One-Pot Synthesis of Imines from Nitroaromatics and Aromatic Alcohols by Transfer Hydrogenation

Hongming Zhang [1,2,3], Jiahe Zhuang [1], Xiangrui Feng [1] and Ben Ma [1,*]

[1] School of Environmental and Chemical Engineering, Jiangsu Ocean University, Lianyungang 222005, China
[2] Jiangsu Institute of Marine Resources Development, Jiangsu Ocean University, Lianyungang 222005, China
[3] School of Safety Science and Emergency Management, Wuhan University of Technology, Wuhan 430070, China
* Correspondence: maben@jou.edu.cn

Abstract: $Co_{0.6}Ni_{0.4}S_2$/rGO catalysts exhibit excellent photocatalytic performance for one-step synthesis of *N*-benzylideneaniline from nitrobenzene and benzyl alcohol by transfer hydrogenation, and the selectivity and yield of *N*-benzylideneaniline can reach as high as 93% and 77.2%, respectively. The reaction process for the synthesis of imines can be divided into two steps: benzyl alcohol is oxidized to benzaldehyde, while nitrobenzene is reduced to aniline; benzaldehyde and aniline are condensed to form imines. Under visible light irradiation, photo-induced electrons in $Co_{0.6}Ni_{0.4}S_2$/rGO photocatalyst play an important role in activating nitrobenzene and benzaldehyde. Photo-induced holes are mainly responsible for the partial dehydrogenation of benzyl alcohol to benzaldehyde. Next, aniline molecules condense with benzaldehyde molecules to synthesize imine. The photocatalytic system provides an environmentally friendly for the synthesis of imines and supplies an alternative approach for hydrogen auto-transfer reactions.

Keywords: imine; photocatalytic; $Co_{0.6}Ni_{0.4}S_2$/rGO; transfer hydrogenation

check for updates

Citation: Zhang, H.; Zhuang, J.; Feng, X.; Ma, B. $Co_{0.6}Ni_{0.4}S_2$/rGO Photocatalyst for One-Pot Synthesis of Imines from Nitroaromatics and Aromatic Alcohols by Transfer Hydrogenation. *Coatings* **2022**, *12*, 1799. https://doi.org/10.3390/coatings12121799

Academic Editor: Emerson Coy

Received: 28 October 2022
Accepted: 21 November 2022
Published: 23 November 2022

1. Introduction

Imines are important building blocks for the synthesis of agrochemical, biologically active compounds, pharmaceutical and fine chemicals [1,2]. Conventionally, imines are synthetized by oxidative dehydrogenation of secondary amines in the presence of molecular oxygen or atmosphere oxygen [3]. The use of O_2 instead of other strong oxidants such as o-iodoxybenzoic acid and chromate not only is more environmentally friendly, but also reduces the cost of the reaction. In addition, high selectivity is readily achieved by dehydrogenation reaction since secondary amines cannot be dehydrogenated into nitriles. However, the steric hindrance around the N-H limits the conversion efficiency of substrates [4]. The synthesis of asymmetric imines is limited because it is difficult to selectively oxidize two types of α-CH with similar properties on asymmetric diphenylamine. Condensation of amines and aldehydes over Lewis acid catalysts is another important method for imines synthesis [5,6]. This route usually needs the assistance of over-stoichiometric amounts of base to form target products. In addition, the instability of reactants under normal conditions (both aldehydes and anilines are easily oxidized by oxygen) also increases the risk of the reaction.

Transfer hydrogenation, a fundamental step in a variety of chemistry processes, involves oxidation and reduction processes [7]. The photocatalytic selective oxidation of benzyl alcohol to benzaldehyde and reduction of nitrobenzene to aniline are typical oxidation and reduction processes, respectively. Therefore, photocatalytic synthesis of imines from aromatic alcohols (the hydrogen donor) and nitroaromatics (the hydrogen acceptor) by transfer hydrogenation is an excellent synthetic strategy, which can not only improve

the utilization of atoms, but also avoid the separation of intermediates. In addition, the substrates used in this synthesis method have a wide range of sources, which can greatly expand the variety of synthetic imines. Up to now, the catalysts currently used in the reaction process include precious metals [8,9], non-noble metal oxides [10] and transition metal compounds [11,12], which exhibit high catalytic activity for one-pot synthesis of imine directly from nitrobenzene and benzyl alcohol by transfer hydrogenation strategy.

Ternary transition metal sulfide semiconductors have received tremendous attention due to their appropriate physical and chemical properties [13], and show excellent photocatalytic performance for photocatalytic pollutants degradation, photocatalytic hydrogen evolution, and photocatalytic carbon dioxide reduction [14–17]. Herein, we report the synthesis of $Co_xNi_{1-x}S_2$/rGO through a facile solvothermal synthesis. The as-prepared noble-metal-free $Co_{0.6}Ni_{0.4}S_2$/rGO material is proved to be a highly active photocatalyst for one-pot system of imines from nitroaromatics and aromatic alcohols.

2. Materials and Methods

2.1. Catalyst Preparation

$Co_{0.6}Ni_{0.4}S_2$/rGO composites were prepared in a hydrothermal autoclave with a 100 mL Teflon lining. Firstly, 3 mmol cobaltous acetate ($Co(CH_3COO)_2{\cdot}4H_2O$), 2 mmol nickel acetate ($Ni(CH_3COO)_2{\cdot}4H_2O$) and 50 mg reduced graphene oxide were dispersed in a mixture of deionized water (20 mL) and ethylene glycol (20 mL). After vigorous stirring for 0.5 h at room temperature, the soliquoid was labeled solution A. Secondly, 5 mmol sodium hyposulfite ($Na_2S_2O_3{\cdot}5H_2O$) and 300 mg oxalic acid ($H_2C_2O_4$) were dispersed in 20 mL of deionized water, and the solution was marked as solution B after stirring for 0.5 h. Next, solution B was slowly dropped into solution A while keeping stirring for another 0.5 h. After that, the soliquoid was transferred into the Teflon-lined hydrothermal autoclave, and maintained at 180 °C. After 18 h, the reaction system was naturally cooled to room temperature. Deionized water and anhydrous ethanol were used to clean the precipitate, respectively. Finally, $Co_{0.6}Ni_{0.4}S_2$/rGO composites were obtained via drying in a vacuum environment at 40 °C for 12 h. By changing the molar ratio of cobalt acetate and nickel acetate in the preparation process, CoS_2/rGO, $Co_{0.8}Ni_{0.2}S_2$/rGO, $Co_{0.4}Ni_{0.6}S_2$/rGO, $Co_{0.2}Ni_{0.8}S_2$/rGO, and NiS_2/rGO catalysts could be obtained under the same condition.

2.2. Catalyst Characterization

The physical and chemical properties of the samples were measured by X-ray diffractometer (XRD, Rigaku D-max/RB, Rigaku, Tokyo, Japan), high resolution transmission electron microscopy (HRTEM, JEM-2100F, Bruker, Billerica, MA, USA), field-emission scanning electron microscopy (FESEM, JSM-5600, Jeol, Tokyo, Japan), X-ray photoelectron spectroscopy (XPS, Kratos XSAM800, Kratos, Manchester, Britain), UV-visible absorption spectrometer (UV-vis, UV-3600, Shimadzu, Tokyo, Japan), fluorescence spectrophotometer (PL, F-700 FL 220–240 eV, Tokyo, Japan) and so on.

2.3. Photocatalytic Synthesis of Imines

The photocatalytic reactions were conducted in a 20 mL Pyrex glass tube under nitrogen atmosphere. In a typical photocatalytic experiment process, 0.5 mmol of nitrobenzene, 1.5 mmol of benzyl alcohol, 40 mg of $Co_{0.6}Ni_{0.4}S_2$/rGO catalysts and 10 mL of toluene were introduced into the glass vessel with at a stirring speed of 300 rpm. The suspension was purged with nitrogen flow for 20 min until an adsorption-desorption equilibrium was established between photocatalytic and reactants. The reaction system was irradiated using a 350 W Xe lamp in a nitrogen atmosphere of 1 atmosphere, and the light intensity of the liquid surface was measured to be 280 mW/cm^2. The reaction temperature was carefully controlled at 90 °C for 6 h by circulating cool water. After reaction, the reaction mixtures were analyzed by a gas chromatograph (Agilent 7820A, Agilent, Santa Clara, CA, USA).

The conversion of reactants, selectivity and yield of target products were calculated following Equations (1)–(3):

$$Conv.(\%) = \frac{C_0 - C_t}{C_0} \times 100\% \quad (1)$$

$$Select.(\%) = \frac{C_p}{C_0 - C_t} \times 100\% \quad (2)$$

$$Yield(\%) = \frac{C_p}{C_0} \times 100\% \quad (3)$$

where C_0 and C_t represent the concentrations of reactant at initial and reaction time t, respectively, and C_p is the concentration of target product. It should be worth noting that the selectivity and yield of imine are calculated based on reduction product of nitrobenzene.

3. Results

3.1. Catalyst Characterization

The surface chemical composition of $Co_{0.6}Ni_{0.4}S_2$/rGO samples were analyzed by the XPS measurements. The main peaks at 854.0, 778.9, 285.0 and 163.1 eV in the survey spectrum are, respectively, attributed to Ni 2p, Co 2p, C 1s and S 2p, proving the co-existence of Co, Ni, S and C in the $Co_{0.6}Ni_{0.4}S_2$/rGO sample (Figure 1A) [15,18]. In the Co 2p XPS spectrum (Figure 1B), two main peaks at 778.6 and 793.6 eV are corresponding to Co $2p_{3/2}$ and Co $2p_{1/2}$ [19]. The binding energies at 780.9 and 797.0 eV can be attributed to Co^{2+} photoelectron peak in cobalt oxide, indicating that a small amount of cobalt is oxidized on the surface [20]. The binding energies of Ni $2p_{3/2}$ (853.3 eV) and Ni $2p_{1/2}$ (870.6 eV) in Ni 2p XPS spectrum (Figure 1C) agree well with the values reported in the previous work [21]. In addition, peaks at 857.0 and 874.5 eV are in accordance with the Ni^{2+} in nickel oxide, indicating that a small amount of nickel is also oxidized on the surface [22]. Figure 1D shows the XPS spectrum of S_2^{2-}, the binding energies at 162.7 and 163.7 eV are the characteristic of S_2^{2-} species in transition metal disulfides, and the binding energies at 161.6 and 169.5 eV, and 165.3 and 171.1 eV are assigned to S^{2-} and SO_4^{2-}, respectively [23–25]. In summary, element Co, Ni and S are mainly in the form of disulphide in sample, and there is a small amount of oxidation state on the surface.

XRD analysis was applied to investigate the crystalline structure of as-prepared samples, and the results are demonstrated in Figure 2A. No obvious diffraction peaks of reduced graphene oxide are observed in all samples. The strong diffraction peaks of CoS_2 are consistent with a cubic phase (JCPDS Card No. 89-1492), implying the purity of as-synthesized CoS_2 [26]. The as-prepared NiS_2/rGO samples are the mixture of NiS/rGO and NiS_2/rGO, which are assigned to a hexagonal phase (JCPDS Card No. 89-1955) and a cubic phase (JCPDS Card No. 88-1709), respectively [27,28]. It is maybe because that NiS_2 is reduced by oxalic acid to NiS. Interestingly, the characteristic diffraction peaks of NiS (30.0, 34.4, 45.5 and 53.2°) disappear in $Co_xNi_{1-x}S_2$/rGO samples. It means that the stability of the sample is improved in the presence of Co. Both physical and chemical similarities of Co and Ni enable the structural compatibility [29]. There are new peaks (38.1 and 50.3°) observed in $Co_xNi_{1-x}S_2$/rGO samples, indicating the formation of solid solutions.

The light-absorbing ability of $Co_{0.6}Ni_{0.4}S_2$ and $Co_{0.6}Ni_{0.4}S_2$/rGO samples were determined by UV-vis diffuse reflectance spectra. $Co_{0.6}Ni_{0.4}S_2$ particles and their composites show strong light absorption in the range of 400–600 nm (Figure 2B). According to the literature, the absorption band in the range of 400–600 nm can be ascribed to the d-d transitions of Co (III) and Ni (III) ions in the catalysts [30]. After the introduction of graphene carrier, the light absorption capacity of $Co_{0.6}Ni_{0.4}S_2$/rGO composites is stronger than that of pure $Co_{0.6}Ni_{0.4}S_2$, indicating that visible light can be exploited more efficient by composites in the presence of rGO [31].

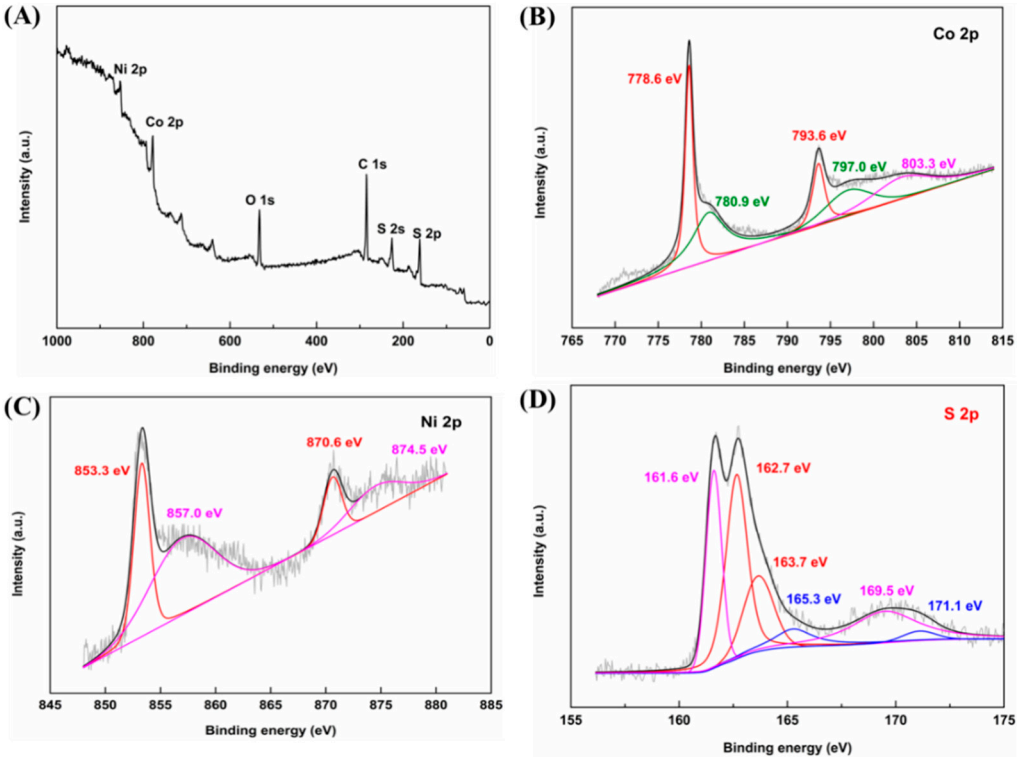

Figure 1. XPS spectra of $Co_{0.6}Ni_{0.4}S_2$/rGO samples: (**A**) the wide-scan XPS spectrum, (**B**) Co 2p, (**C**) Ni 2p, (**D**) S 2p.

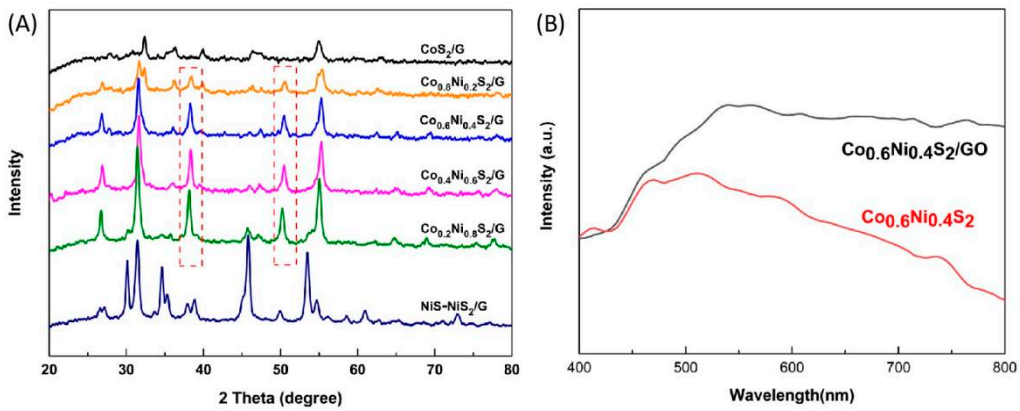

Figure 2. XRD pattern of $Co_xNi_{1-x}S_2$/rGO (x = 0, 0.2, 0.4, 0.6, 0.8 and 1) (**A**), and UV-vis diffuse reflectance spectra of $Co_{0.6}Ni_{0.4}S_2$ and $Co_{0.6}Ni_{0.4}S_2$/rGO samples (**B**).

TEM and SEM are common tools for researchers to study the crystal structure and microstructure of solid catalysts. Figure 3 shows representative field-emission scanning electron microscopy (FESEM) images of $Co_{0.6}Ni_{0.4}S_2$/rGO sample. From Figure 3A, $Co_{0.6}Ni_{0.4}S_2$/rGO subspheroidal particles with an average particle size of about 400 nm are well distributed on the surface of graphene, and the interplanar crystal spacing is 0.24 nm. Figure 3B is the FESEM of $Co_{0.6}Ni_{0.4}S_2$ subspheroidal particles, and the surface of particles is particularly rough. It can be explained that samples are etched by oxalic acid during the preparation. The rough surface not only increases the surface area, but also provides more adsorption and active positions for the reactants, which can help improve the catalytic activity. It can be observed that Co, Ni and S elements distribute almost uniformly in the surface of $Co_{0.6}Ni_{0.4}S_2$ from the elemental distribution maps of Co, Ni and S (Figure A1A–D), consistent with the EDX results (Figure A2).

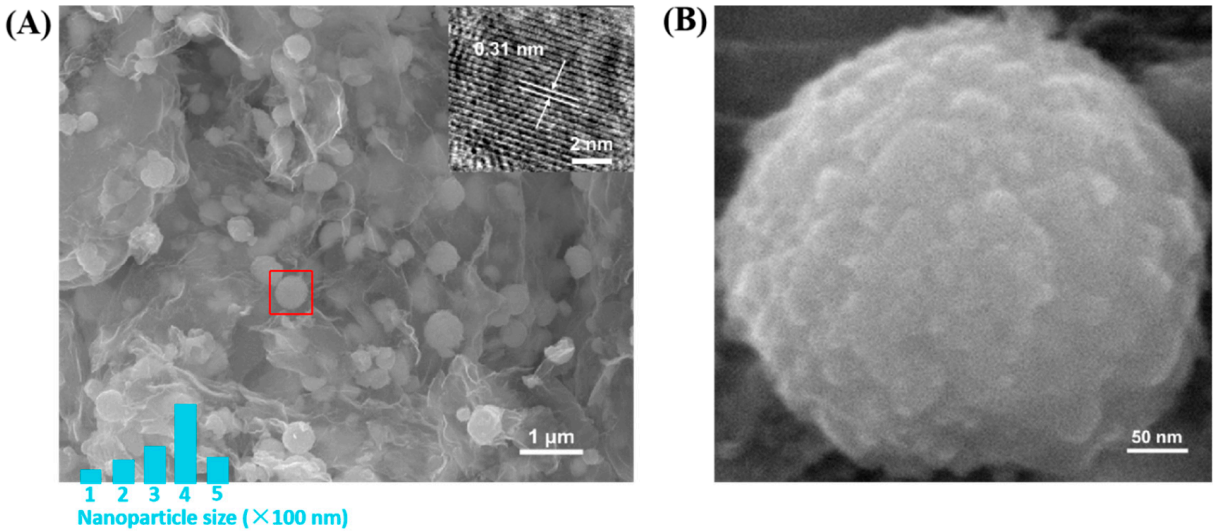

Figure 3. SEM images (**A**,**B**) of $Co_{0.6}Ni_{0.4}S_2$/rGO, and the inset pictures in picture (**A**) are the size distributions of $Co_{0.6}Ni_{0.4}S_2$ particles and HRTEM images.

3.2. The Performance of Photocatalytic Synthesis of Imines

The photocatalytic performances of various catalysts for the synthesis of *N*-benzylideneaniline from nitrobenzene and benzyl alcohol were tested (Figure 4). It is clear that catalysts have greatly affected the yield of *N*-benzylideneaniline from Table 1. No imines are detected using pure graphene as photocatalytic (entry1 Table 1). CoS_2/rGO and NiS_2/rGO show poor photocatalytic activity under the giving conditions and the yields of *N*-benzylideneaniline are only 32.2 and 27.9%, respectively (entries 2 and 7, Table 1). Expectedly, all $Co_xNi_{1-x}S_2$/rGO catalysts show better photocatalytic activity for the synthesis of *N*-benzylideneaniline than that of pure CoS_2/rGO and NiS_2/rGO catalysts. In addition, the highest yield of *N*-benzylideneaniline (77.2%) is achieved over $Co_{0.6}Ni_{0.4}S_2$/rGO sample (entry 4, Table 1). Therefore, $Co_{0.6}Ni_{0.4}S_2$/rGO is used as the catalyst for the following experiments. For comparison, the reaction was conducted without light irradiation (entry 8, Table 1), and the yield of *N*-benzylideneaniline is only 29.1%. This phenomenon shows that the light plays a significant role in this reaction under the giving conditions.

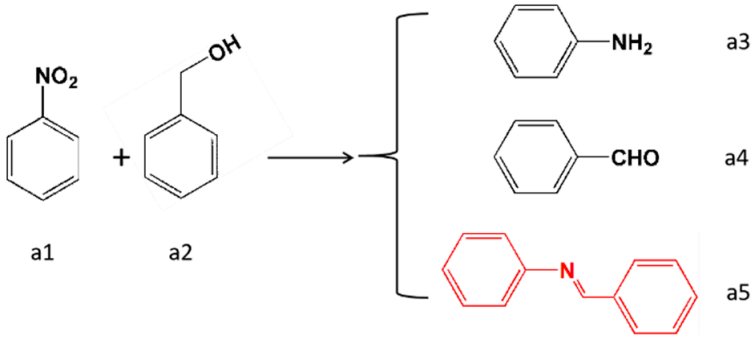

Figure 4. Photocatalytic One-Pot Synthesis of Imine from Nitrobenzene and Benzyl alcohol.

The conversion of nitrobenzene, the selectivity of aniline, *N*-benzylideneaniline and *N*-phenylbenzylamine dependence on the irradiation intensity are shown in Figure 5. Nitrobenzene is first converted to aniline, and the higher of light intensity results in the higher conversion of nitrobenzene under the same reaction conditions. When the light intensity exceeds 280 mW/cm^2, most of the aniline has been converted into imine. It is worth noting that no imine is detected when the light intensity is less than 320 mW/cm^2. However, increasing the intensity of light from 320 to 360 mW/cm^2, the selectivity of *N*-phenylbenzylamine rises obviously, suggesting that a part of *N*-benzylideneaniline has been reduced to *N*-phenylbenzylamine in reaction process. When the intensity of light is

enhanced, more photo-generated electrons can be transferred to higher energy level, and have enough energy to overcome the energy barrier of *N*-phenylbenzylamine synthesis, resulting in the increase of *N*-phenylbenzylamine selectivity. Obviously, the energy barrier of *N*-benzylideneaniline synthesis is less than that of *N*-phenylbenzylamine synthesis from *N*-benzylideneaniline.

Table 1. Experimental results of photocatalytic synthesis of *N*-benzylideneaniline over $Co_xNi_{1-x}S_2$/rGO (x = 1, 0.8, 0.6, 0.4, 0.2 and 0) catalyst.

Entry	Catalyst	Conv.(%)		Select. (%)		Yield (%)
		a1	a2	a3	a5	a5
1	rGO	1	14	0	0	0
2	CoS_2/rGO	62	76	44	52	32.2
3	$Co_{0.8}Ni_{0.2}S_2$/rGO	77	83	9	88	67.8
4	$Co_{0.6}Ni_{0.4}S_2$/rGO	83	91	6	93	77.2
5	$Co_{0.4}Ni_{0.6}S_2$/rGO	74	79	11	86	63.6
6	$Co_{0.2}Ni_{0.8}S_2$/rGO	57	62	20	77	43.9
7	NiS_2/rGO	41	55	27	68	27.9
8 [a]	$Co_{0.6}Ni_{0.4}S_2$/rGO	35	44	15	83	29.1

[a] The reaction was conducted without light irradiation.

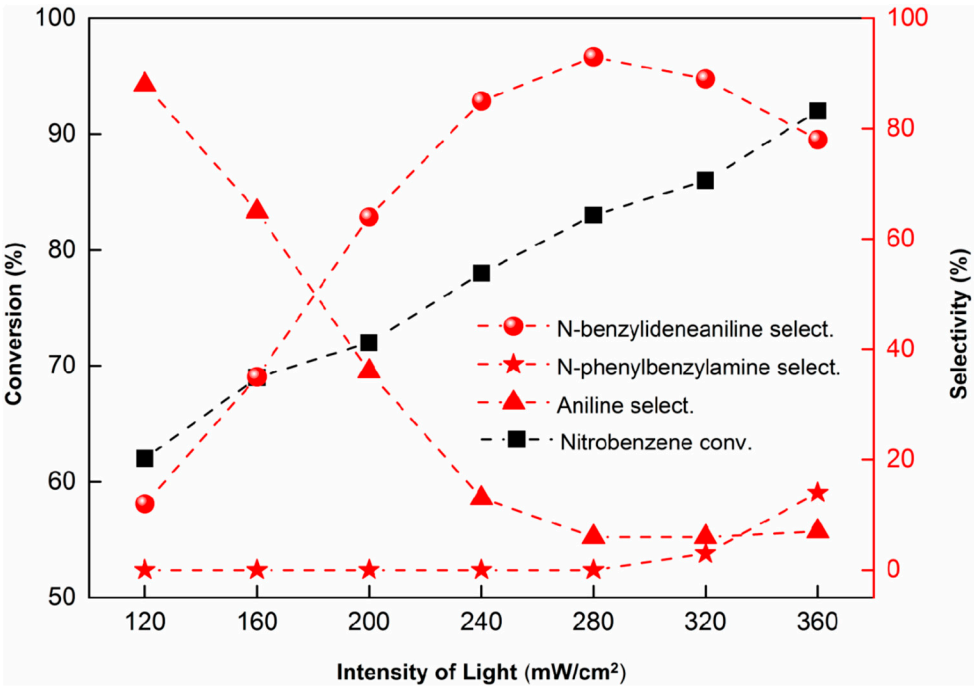

Figure 5. The dependence of photocatalytic activity for *N*-benzylideneaniline synthesis on the irradiation intensity over $Co_{0.6}Ni_{0.4}S_2$/rGO.

3.3. Impact of Solvent on Photocatalytic Activity

Generally speaking, there is an important influence on photocatalytic activity for solvents [32,33]. The reaction of imines synthesis was conducted in various solvent. Non-polar solvents promote the synthesis of imines, and yield of imines are 77.2% and 76.5% in toluene and mesitylene (entries1 and 2, Table 2), respectively. Interestingly, both the conversion of reactants and selectivity of imine are suppressed in polar solvents (entries 3–5, Table 2). It can be explained that the solvent with high polarity index has a large interaction with the reaction substrates, which weakens the interaction between the substrates and the catalysts, thus reducing the catalytic activity [34]. For condensation process, -NH_2 in aniline and -CHO in benzaldehyde are less nucleophilic and electrophilic in polar solvents than

that in non-polar solvents [35]. Therefore, imines are more easily synthesized in nonpolar solvents. In addition, the by-product water also has a great influence on the reaction. When 30 mg of anhydrous magnesium sulfate ($MgSO_4$) was added to THF and ethanol solvent, respectively, both the conversion of reactants and yield of *N*-benzylideneaniline enhances gradually (entries 7 and 8, Table 2). However, the adding of $MgSO_4$ has little effect on the reaction in toluene (entry 6, Table 2). This may be because $MgSO_4$ can remove water dissolved in the solvent, resulting in the reaction proceeds in the positive direction. In other words, synthesis of imine from condensation of amines and aldehydes is reversible reaction.

Table 2. The performances of photocatalytic synthesis of *N*-benzylideneaniline in various solvents.

Entry	Solvent	Conv.(%)		Select. (%)	Yield (%)
		Nitrobenzene	Benzyl Alcohol	Imine	Imine
1	Toluene	83	91	93	77.2
2	Mesitylene	85	94	90	76.5
3	THF	69	76	58	40.0
4	Ethanol	35	42	19	6.7
5	Water	11	25	-	Trace
6 [a]	Toluene	85	95	94	79.9
7 [a]	THF	82	88	71	58.2
8 [a]	Ethanol	49	55	32	15.7

[a] 30 mg of anhydrous magnesium sulfate ($MgSO_4$) was added to the reaction.

3.4. Reductive Coupling of Several Other Substrates to Imine

To demonstrate the general applicability of the $Co_{0.6}Ni_{0.4}S_2$/rGO photocatalyst, the synthesis of imines from a wide range of aromatic alcohols and nitroarenes were investigated (Figure 6), and results are summarized in Table 3. It can be seen that substituent groups on reactant have significantly affected both selectivity and yield of imines. For instance, when nitrobenzene reacts with p-chlorophenyl alcohol or 3-bromobenzyl alcohol, the conversations of nitrobenzene and aromatic alcohols, and the yield of target products are higher than that in the reaction system of benzyl alcohol and nitrobenzene (entries 1 and 2, Table 3). The functional groups with strong electronegativity contribute to the synthesis of imines [11]. However, substitutions with electron-donating (-CH_3, -CH_2CH_3) on aromatic alcohols exhibit poor both conversion of reactant and yield of imines, and the yields are only 59.3 and 22.4%, respectively (entries 3 and 4, Table 3). When nitroaromatics reacts with benzyl alcohol, electron-withdrawing groups (-Cl and -Br) have slight effect on both conversion of reactants and yield of imines (entries 5 and 6, Table 3), and electron-donating group (-CH_3) shows poor selectivity of imine (entry 7, Table 3). For the nitroaromatics and p-substituted benzyl alcohols coupled system, substitutions with electron-donating and electron-withdrawing inhibit the occurrence of coupling reaction, and the selectivity of imines are significantly reduced (entries 8 and 9, Table 3). In a word, $Co_{0.6}Ni_{0.4}S_2$/rGO catalysts show the high yield of other imines from nitroaromatics and aromatic alcohols.

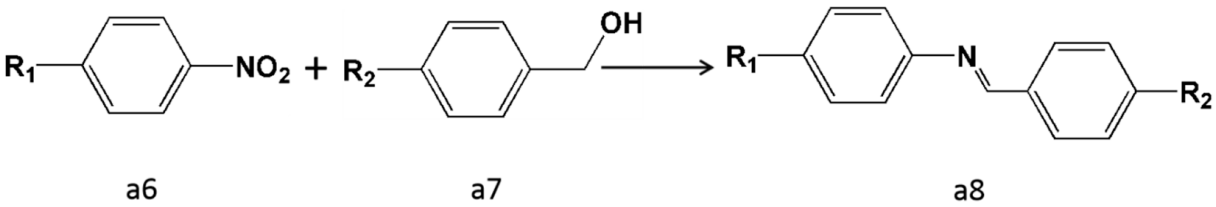

Figure 6. Photocatalytic One-Pot Synthesis of Imine from Nitroaromatics and Aromatic Alcohols.

Table 3. The photocatalytic synthesis of Imine from several other substrates over the $Co_{0.6}Ni_{0.4}S_2$/rGO catalyst.

Entry	Reactant		Conv. (%)		Select. (%)	Yield (%)
	R_1	R_2	a6	a7	a8	a8
1	H	Cl	90	99	94	84.6
2	H	Br	85	94	91	77.4
3	H	CH_3	69	77	86	59.3
4	H	CH_3CH_2	51	60	44	22.4
5	Cl	H	82	96	92	75.4
6	Br	H	80	93	94	75.2
7	CH_3	H	93	97	80	74.4
8	Cl	Cl	88	94	63	55.4
9	CH_3	CH_3	66	70	54	35.6

3.5. Stability of Catalyst

Stability is an important criterion to evaluate the properties of heterogeneous catalysts. According to our previous research, the activity of transition metal sulfides is greatly reduced after several cycles, such as FeS_2 and CoS_2. In our work, the $Co_{0.6}Ni_{0.4}S_2$/rGO catalyst shows better stability for synthesis of *N*-benzylideneaniline after five successive reactions under the protection of graphene (Figure 7). FESEM analysis was performed on the catalyst for recycled catalysts. As can be seen from Figure A3, there are no significant changes observed for $Co_{0.6}Ni_{0.4}S_2$/rGO catalysts in synthesis of *N*-benzylideneaniline.

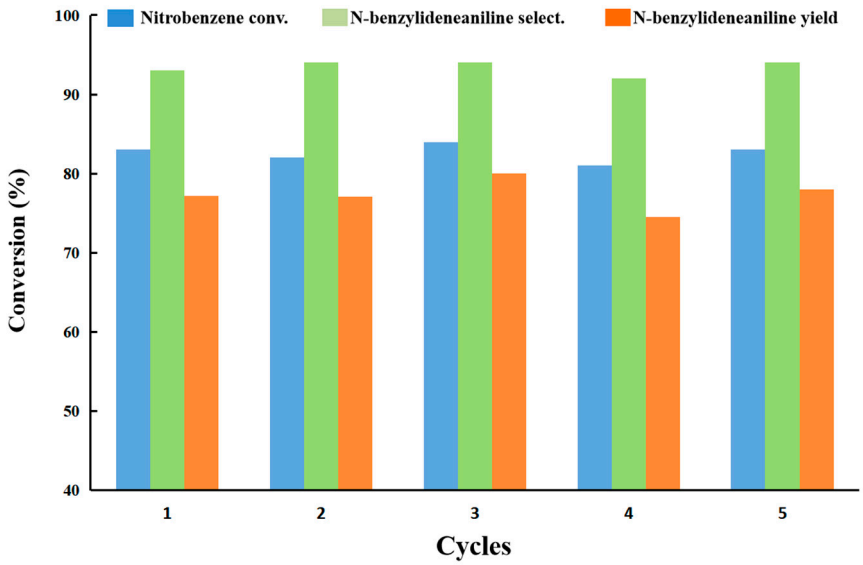

Figure 7. Photocatalytic stability of $Co_{0.6}Ni_{0.4}S_2$/rGO in five cycles for synthesis of *N*-benzylideneaniline.

3.6. Proposed Mechanism

As a semiconductor material, $Co_{0.6}Ni_{0.4}S_2$ can produce photo-generated electrons and holes under visible light illumination. This phenomenon has been proved by photoluminescence (PL) spectra of $Co_{0.6}Ni_{0.4}S_2$ and $Co_{0.6}Ni_{0.4}S_2$/rGO (Figure 8). When photo-generated electrons are excited from its valence band (VB) to conduction band (CB), photo-generated holes are left at the VB. In addition, graphene can effectively suppress the recombination of photo-generated electrons and holes [25]. In order to investigate the photocatalytic mechanism for imines synthesis by transfer hydrogenation, the scavenger of electrons (5,5-dimethyl-1-pyrroline *N*-oxide, DMPO) and holes (triethanolamine, TEA) were added to the experiment. When 1.0 mL of DMPO was employed to trap the photogenerated electrons of $Co_{0.6}Ni_{0.4}S_2$, the conversion of nitrobenzene decreased sharply from 83% to 26%, and the conversion of benzyl alcohol increased from 91% to 98%, which can be explained that

more photo-generated holes can participate in the dehydrogenation of aromatic alcohols to aromatic aldehydes. Adding 1.0 mL of TEA to the reaction system, the conversion of benzyl alcohol and nitrobenzene decreased to 38% and 21%, respectively, which is almost the same as that in the dark reaction (Figure 9). On the basis of the results described above, it can be speculated that the dehydrogenation of benzyl alcohol is the prerequisite reaction, and protons (H^+) liberated in the dehydrogenation reaction are used as hydrogen sources for reducing nitrobenzene effectively to aniline.

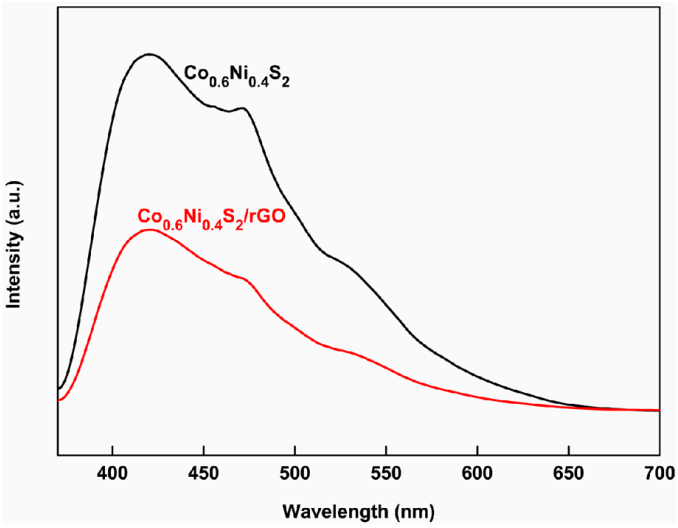

Figure 8. Photoluminescence spectra of $Co_{0.6}Ni_{0.4}S_2$ and $Co_{0.6}Ni_{0.4}S_2$/rGO (excitation wavelength, 280 nm).

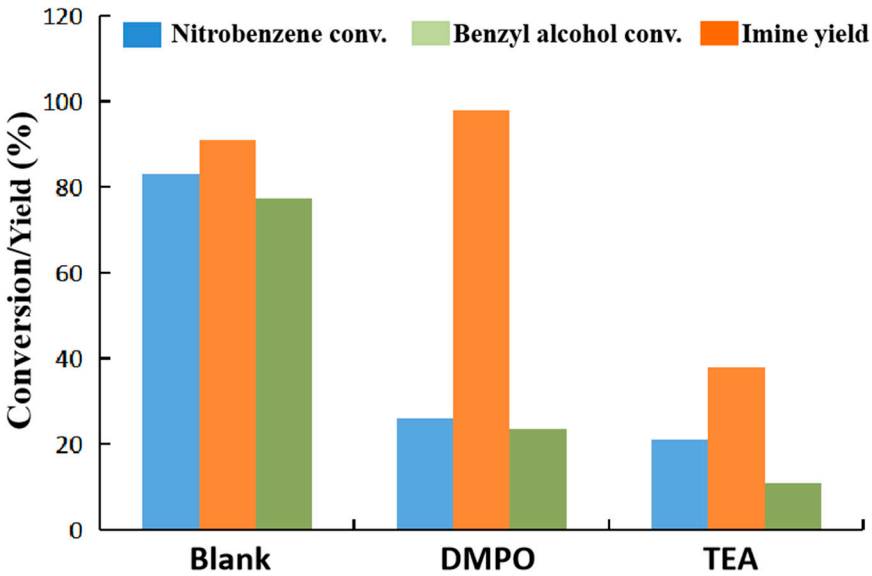

Figure 9. The conversions of nitrobenzene and benzyl alcohol, and the yield of imine by adding different additives.

Using aniline (1 mmol) and benzaldehyde (1 mmol) as reactants, the conversion of aniline was 74% in the same reaction condition for 3 h. When 0.8 mL of TEA was added to the reaction, the conversion of aniline was reduced to 46%. By changing the amount of benzaldehyde, the initial concentration ratio of benzaldehyde and aniline can be adjusted to 0.2, 0.5, 1.5 and 2. In addition, the addition of TEA had little effect on reaction of the initial concentration ratio of 0.2 and 0.5 (Figure 10). However, TEA could significantly reduce the conversion of the reaction, when the initial concentration ratio was 1.5 and 2. On the

contrary, adding 0.9 mL of DMPO to the reaction which the initial concentration ratio was 0.2, 0.5 and 1, the conversion of aniline was significantly lower than the blank experiment. However, DMPO had little effect on the reaction which the initial concentration ratio was 1.5 and 2.

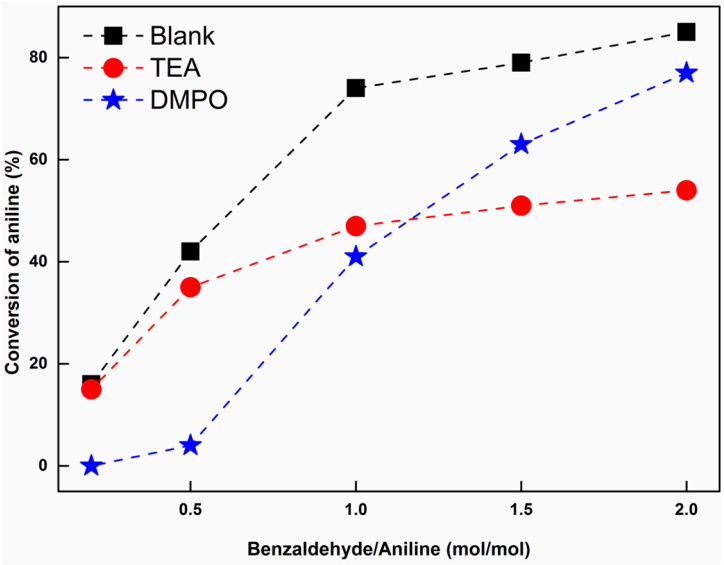

Figure 10. The conversions of nitrobenzene and benzyl alcohol, and the yield of imine by adding different additives.

According to the reaction formula, the amount of aniline and benzaldehyde needed for the formation of imine is the same. When an amount of TEA is added to reaction, a part of photo-generated hole is trapped, and the activation of aniline is inhibited, resulting in reducing the conversion of aniline. This phenomenon is especially obvious in the reaction of benzaldehyde excess. On the contrary, DMPO can inhibit the activation of benzaldehyde by capturing photo-generated electrons, which has a great negative impact on the reaction of aniline excess. Therefore, the reaction process for the synthesis of imines from nitrobenzene and benzyl alcohol by hydrogen transfer can be divided into two steps: in the first step, under the action of photo-generated electron and hole, benzyl alcohol is dehydrated to benzaldehyde, while nitrobenzene is reduced to aniline; in the second step, benzaldehyde and aniline are condensed to synthesize imines.

4. Conclusions

The present work demonstrates a novel photocatalytic route for one-step synthesis of imines from nitroaromatics and aromatic alcohol by transfer hydrogenation using $Co_{0.6}Ni_{0.4}S_2$/rGO catalyst. Under visible light irradiation, the reaction for the synthesis of imines can be divided into two steps. Benzyl alcohol is oxidized to benzaldehyde, while nitrobenzene is reduced to aniline; meanwhile, benzaldehyde and aniline are condensed to synthesize imines. The photo-induced electrons in $Co_{0.6}Ni_{0.4}S_2$/rGO photocatalyst play an important role in activating nitrobenzene and benzaldehyde. Photo-induced holes are mainly responsible for the partial oxidation of benzyl alcohol to benzaldehyde, and the H^+ liberated are used as hydrogen sources to reduce photo-induced electrons activated nitrobenzene to aniline. Next, aniline molecules condense with benzaldehyde molecules to synthesize imine. Under the synergistic action of electrons and holes, $Co_{0.6}Ni_{0.4}S_2$/rGO photocatalyst shows good stability, commendable activity and excellent selectivity, and the yield *N*-benzylideneaniline can reach as high as 77.2%. As a dynamic equilibrium process, the removal of by-product water is helpful to improve the yield of imine. The photocatalytic system provides an environmentally friendly and effective pathway for the synthesis of imines, and also supplies an alternative approach for hydrogen auto-transfer reactions.

Author Contributions: Methodology, H.Z. and B.M.; software, J.Z. and X.F.; investigation, J.Z. and X.F.; writing—original draft preparation, H.Z.; writing—review and editing, H.Z. and B.M.; funding acquisition, H.Z. and B.M. All authors have read and agreed to the published version of the manuscript.

Funding: This work was financially supported by Natural Science Foundation of Jiangsu Province (Grant No. BK20201030), Open Research Fund of Jiangsu Institute of Marine Resources Development (Grant No. JSIMR202118), Open-end Funds of Jiangsu Key Laboratory of Function Control Technology for Advanced Materials, Jiangsu Ocean University (Grant No. jsklfctam201807).

Institutional Review Board Statement: Not applicable.

Informed Consent Statement: Not applicable.

Data Availability Statement: All data that support the findings of this study are included within the article.

Conflicts of Interest: The authors declare no conflict of interest.

Appendix A.

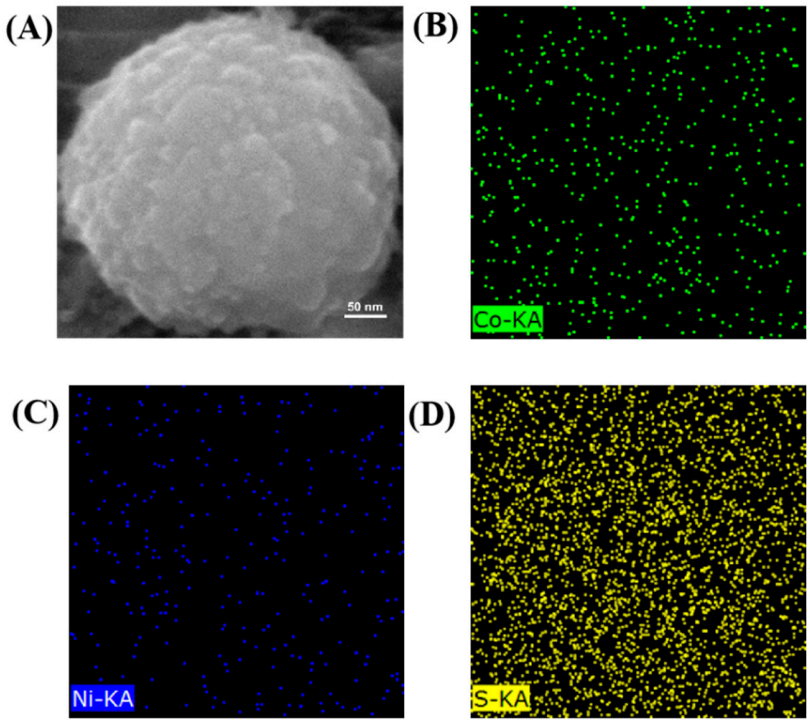

Figure A1. SEM image (**A**) and the elemental distribution maps of Co (**B**), Ni (**C**) and S (**D**) of $Co_{0.6}Ni_{0.4}S_2$/rGO.

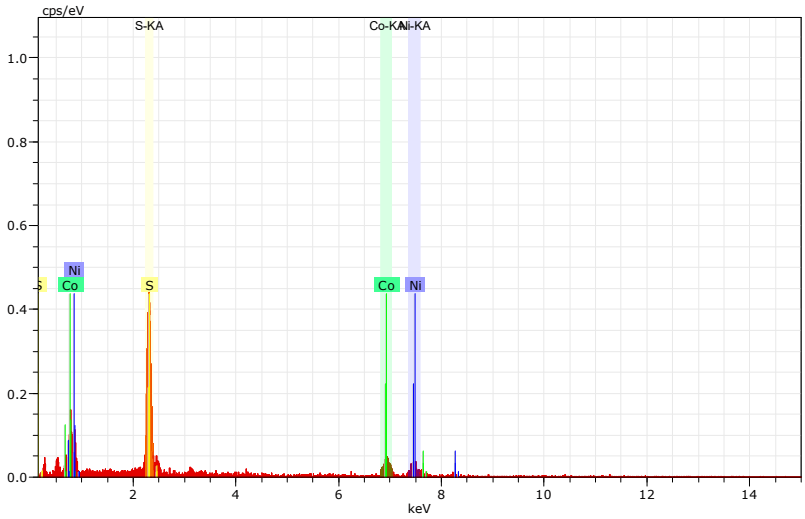

Figure A2. EDX spectra of $Co_{0.6}Ni_{0.4}S_2$/rGO sample.

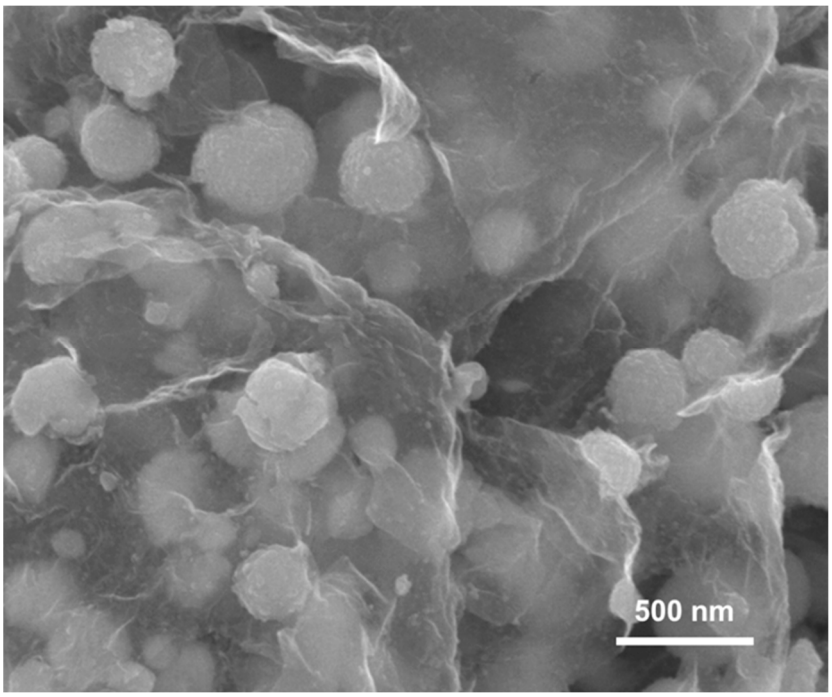

Figure A3. FESEM images of recycled $Co_{0.6}Ni_{0.4}S_2$/rGO catalysts in synthesis of imine.

References

1. Liu, D.; Yang, P.; Zhang, H.; Liu, M.J.; Zhang, W.F.; Xu, D.M.; Gao, J. Direct reductive coupling of nitroarenes and alcohols catalysed by Co-N-C/CNT@AC. *Green Chem.* **2019**, *21*, 2129–2137. [CrossRef]
2. Zhou, P.; Zhang, Z.H. One-pot Reductive Amination of carbonyl Compounds with Nitro Compounds by Transfer Hydrogenation over Co-N_x as catalyst. *ChemSusChem* **2017**, *10*, 1892–1897. [CrossRef] [PubMed]
3. Chen, P.Q.; Guo, Z.F.; Liu, X.; Lv, H.; Che, Y.; Bai, R.; Cui, Y.H.; Xing, H.Z. A visible-light-responsive metal-organic framework for highly efficient and selective photocatalytic oxidation of amines and reduction of nitroaromatics. *J. Mater. Chem. A* **2019**, *7*, 27074–27080. [CrossRef]
4. Chen, B.; Wang, L.Y.; Gao, S. Recent Advances in Aerobic Oxidation of Alcohols and Amines to Imines. *ACS Catal.* **2015**, *5*, 5851–5876. [CrossRef]
5. Zhang, B.; Guo, X.W.; Liang, H.J.; Ge, H.B.; Gu, X.M.; Chen, S.; Yang, H.M.; Qin, Y. Tailoring Pt-Fe_2O_3 interfaces for selective reductive coupling reaction to synthesize imine. *ACS Catal.* **2016**, *6*, 6560–6566. [CrossRef]
6. Ch, V.; Sandupatla, R.; Lingareddy, E.; Raju, D. One-pot synthesis of imines by direct coupling of alcohols and amines over magnetically recoverable $CdFe_2O_4$ nanocatalyst. *Mater. Lett.* **2021**, *302*, 130417. [CrossRef]

7. Yang, H.M.; Cui, X.J.; Dai, X.C.; Deng, Y.Q.; Shi, F. Carbon-catalysed reductive hydrogen atom transfer reactions. *Nat. Commun.* **2015**, *6*, 6478. [CrossRef] [PubMed]
8. Sahoo, D.P.; Patnaik, S.; Rath, D.; Mohapatra, P.; Mohanty, A.; Parida, K. Influence of Au/Pd alloy on an amine functionalised ZnCr LDH-MCM-41 nanocomposite: A visible light sensitive photocatalyst towards one-pot imine synthesis. *Catal. Sci. Technol.* **2019**, *9*, 2493–2513. [CrossRef]
9. Sankar, M.; He, Q.; Dawson, S.; Nowicka, E.; Lu, L.; Bruijnincx, P.C.A.; Beale, A.M.; Kiely, C.J.; Weckhuysen, B.M. Supported bimetallic nano-alloys as highly active catalysts for the one-pot tandem synthesis of imines and secondary amines from nitrobenzene and alcohols. *Catal. Sci. Technol.* **2016**, *6*, 5473–5482. [CrossRef]
10. Hirakawa, H.; Katayama, M.; Shiraishi, Y.; Sakamoto, H.; Wang, K.; Ohtani, B.; Ichikawa, S.; Tanaka, S.; Hirai, T. One-Pot Synthesis of Imines from Nitroaromatics and Alcohols by Tandem Photocatalytic and Catalytic Reactions on Degussa (Evonik) P25 Titanium Dioxide. *ACS Appl. Mater. Interfaces* **2015**, *7*, 3797–3806. [CrossRef]
11. Wu, Y.H.; Ye, X.J.; Zhang, S.J.; Meng, S.G.; Fu, X.L.; Wang, X.C.; Zhang, X.M.; Chen, S.F. hotocatalytic synthesis of Schiff base compounds in the coupled system of aromatic alcohols and nitrobenzene using $Cd_XZn_{1-X}S$ photocatalysts. *J. Catal.* **2018**, *359*, 151–160. [CrossRef]
12. Ye, X.; Chen, Y.; Lin, C.; Ding, R.; Wang, X.; Zhang, X.; Chen, S. One-pot synthesis of Schiff base compounds via photocatalytic reaction in the coupled system of aromatic alcohols and nitrobenzene using $CdIn_2S_4$ photocatalyst. *Dalton Trans.* **2018**, *47*, 10915–10924. [CrossRef] [PubMed]
13. Qin, J.F.; Yang, M.; Chen, T.S.; Dong, B.; Hou, S.; Ma, X.; Zhou, Y.Z.; Yang, X.L.; Nan, J.; Chai, Y.M. Ternary metal sulfides MoCoNiS derived from metal organic frameworks for efficient oxygen evolution. *Int. J. Hydrog. Energ.* **2020**, *45*, 2745–2753. [CrossRef]
14. Huang, D.L.; Wen, M.; Zhou, C.Y.; Li, Z.H.; Cheng, M.; Chen, S.; Xue, W.J.; Lei, L.; Yang, Y.; Xiong, W.P.; et al. $Zn_xCd_{1-x}S$ based materials for photocatalytic hydrogen evolution, pollutants degradation and carbon dioxide reduction. *Appl. Catal. B-Environm.* **2020**, *267*, 118651. [CrossRef]
15. Dai, D.S.; Xu, H.; Ge, L.; Han, C.C.; Gao, Y.Q.; Li, S.S.; Lu, Y. In-situ synthesis of CoP co-catalyst decorated $Zn_{0.5}Cd_{0.5}S$ photocatalysts with enhanced photocatalytic hydrogen production activity under visible light irradiation. *Appl. Catal. B-Environm.* **2017**, *217*, 429–436. [CrossRef]
16. Liu, X.L.; Liang, X.Z.; Wang, P.; Huang, B.B.; Qin, X.Y.; Zhang, X.Y.; Dai, Y. Highly efficient and noble metal-free NiS modified $Mn_xCd_{1-x}S$ solid solutions with enhanced photocatalytic activity for hydrogen evolution under visible light irradiation. *Appl. Catal. B-Environm.* **2017**, *203*, 282. [CrossRef]
17. Yang, S.P.; Zhang, C.H.; Cai, Y.Q.; He, X.W.; Niu, H.Y. Synthesis of $Cd_xZn_{1-x}S@Fe_3S_4$ magnetic photocatalyst nanoparticles for the photodegradation of methylene blue. *J. Alloys Compd.* **2018**, *735*, 1955–1961. [CrossRef]
18. Zhang, H.H.; Guan, B.; Gu, J.N.; Li, Y.; Ma, C.; Zhao, J.; Wang, T.Y.; Cheng, C.J. One-step synthesis of nickel cobalt sulphides particles: Tuning the composition for high performance supercapacitors. *RSC Adv.* **2016**, *6*, 58916–58924. [CrossRef]
19. Liu, Y.R.; Shang, X.; Gao, W.K.; Dong, B.; Chi, J.Q.; Li, X.; Yan, K.L.; Chai, Y.M.; Liu, Y.Q.; Liu, C.G. Ternary CoS_2/MoS_2/RGO electrocatalyst with CoMoS phase for efficient hydrogen evolution. *Appl. Surf. Sci.* **2017**, *412*, 138–145. [CrossRef]
20. Li, Y.H.; Cao, L.J.; Qiao, L.; Zhou, M.; Yang, Y.; Xiao, P.; Zhang, Y.H. Ni-Co sulfide nanowires on nickel foam with ultrahigh capacitance for asymmetric Supercapacitors. *J. Mater. Chem. A* **2014**, *2*, 6540–6548. [CrossRef]
21. Shang, X.; Li, X.; Hu, W.H.; Dong, B.; Liu, Y.R.; Han, G.Q.; Chai, Y.M.; Liu, Y.Q.; Liu, C.G. In situ growth of Ni_xS_y controlled by surface treatment of nickel foam as efficient electrocatalyst for oxygen evolution reaction. *Appl. Surf. Sci.* **2016**, *378*, 15–21. [CrossRef]
22. Yang, F.; Yao, J.Y.; He, H.C.; Zhou, M.; Xiao, P.; Zhang, Y.H. Ni-Co oxides nanowire arrays grown on ordered TiO_2 nanotubes with high performance in supercapacitors. *J. Mater. Chem. A* **2013**, *1*, 594–601. [CrossRef]
23. Ma, B.; Tong, X.L.; Guo, C.X.; Guo, X.N.; Guo, X.Y.; Keil, F.J. Pyrite Nanoparticles: An Earth-Abundant Mineral Catalyst for Activation of Molecular Hydrogen and Hydrogenation of Nitroaromatics. *RSC Adv.* **2016**, *6*, 55220–55224. [CrossRef]
24. Ji, N.; Wang, X.Y.; Werdenthaler, C.; Spliethoff, B.; Rinaldi, R. Iron(II) Disulfides as Precursors of Highly Selective Catalysts for Hydrodeoxygenation of Dibenzyl Ether into Toluene. *ChemCatChem* **2015**, *7*, 960–966. [CrossRef]
25. Cai, Y.F.; Pan, Y.G.; Xue, J.Y.; Sun, Q.F.; Su, G.Z.; Li, X. Comparative XPS study between experimentally and naturally weathered pyrites. *Appl. Surf. Sci.* **2009**, *255*, 8750–8760. [CrossRef]
26. Ma, B.; Wang, Y.Y.; Tong, X.L.; Guo, X.N.; Zheng, Z.F.; Guo, X.Y. Graphene-supported CoS_2 Particles: An Efficient Photocatalyst for Selective Hydrogenation of Nitroaromatics in Visible Light. *Catal. Sci. Technol.* **2017**, *7*, 2805–2812. [CrossRef]
27. Surendran, S.; Sankar, K.V.; Berchmans, L.J.; Selvan, R.K. Polyol synthesis of α-NiS particles and its physico-chemical Properties. *Mat. Sci. Semicon. Proc.* **2015**, *33*, 16–23. [CrossRef]
28. Luo, P.; Zhang, H.J.; Liu, L.; Zhang, Y.; Deng, J.; Xu, C.H.; Hu, N.; Wang, Y. Targeted synthesis of unique nickel sulfides (NiS, NiS_2) microarchitectures and the applications for the enhanced water splitting system. *ACS Appl. Mater. Interfaces* **2017**, *9*, 2500–2508. [CrossRef]
29. Chen, G.; Liaw, S.S.; Li, B.S.; Xu, Y.; Dunwell, M.; Deng, S.G.; Fan, H.Y.; Luo, H.M. Microwave-assisted synthesis of hybrid $Co_xNi_{1-x}(OH)_2$ nanosheets: Tuning the composition for high performance supercapacitor. *J. Power Sources* **2014**, *251*, 338–343. [CrossRef]
30. Huirache-Acuña, R.; Pawelec, B.; Rivera-Muñoz, E.M.; GuilLópez, R.; Fierro, J.L.G. Characterization and HDS activity of sulfided Co-Mo-W/SBA-16 catalysts: Effects of P addition and Mo/(Mo + W) ratio. *Fuel* **2017**, *198*, 145–158. [CrossRef]

31. Du, J.M.; Wang, H.M.; Yang, M.K.; Li, K.D.; Zhao, L.X.; Zhao, G.Y.; Li, S.J.; Gu, X.L.; Zhou, Y.L.; Wang, L.; et al. Pyramid-like CdS nanoparticles grown on porous TiO2 monolith: An advanced photocatalyst for H_2 production. *Electrochim. Acta* **2017**, *250*, 99–107. [CrossRef]
32. Ferguson, C.T.J.; Huber, N.; Kuckhoff, T.; Zhang, K.; Landfester, K. Dispersible porous classical polymer photocatalysts for visible light-mediated production of pharmaceutically relevant compounds in multiple solvents. *J. Mater. Chem. A* **2020**, *8*, 1072–1076. [CrossRef]
33. Ma, B.; Wang, Y.Y.; Guo, X.N.; Tong, X.L.; Liu, C.; Wang, Y.W.; Guo, X.Y. Photocatalytic synthesis of 2,5-diformylfuran from 5-hydroxymethyfurfural or fructose over bimetallic Au-Ru nanoparticles supported on reduced graphene oxides. *Appl. Catal. A-Gen.* **2018**, *552*, 70–76. [CrossRef]
34. Ma, J.J.; Yu, X.J.; Liu, X.L.; Li, H.Y.; Hao, X.L.; Li, J.Y. The preparation and photocatalytic activity of Ag-Pd/g-C_3N_4 for the coupling reaction between benzyl alcohol and aniline. *Mol. Catal.* **2019**, *476*, 110533. [CrossRef]
35. Nakai, Y.; Azuma, M.; Muraoka, M.; Kobayashi, H.; Higashimoto, S. One-pot imine synthesis from benzylic alcohols and nitrobenzene on CdS-sensitized TiO_2 photocatalysts: Effects of the electric nature of the substituent and solvents on the photocatalytic activity. *Mol. Catal.* **2017**, *443*, 203–208. [CrossRef]